

# Infrared and Raman Spectra for Complexes of Small Cationic Gold Clusters and Hydrogen Sulphide

G.P. Li and I.P. Hamilton\*

Contribution from: Department of Chemistry, Wilfrid Laurier University, Waterloo, Canada N2L 3C5

Received: October 19, 2004

Accepted (in revised form): October 30, 2004

## Résumé

*Nous avons calculé les spectres infrarouge et Raman des complexes de clusters cationiques de l'or  $Au_n^+$  ( $n = 1-4$ ) et de  $H_2S$  en utilisant la théorie de densité fonctionnelle. Les intensités des bandes spectrales de  $H_2S$  sont significativement amplifiées par la formation de complexe pour les spectres infrarouge ainsi que Raman. Les déplacements des bandes spectrales de  $H_2S$  sont corrélés avec les changements dans les géométries et les énergies de liaison des complexes et avec le transfert de charge lié à la formation du complexe.*

## Abstract

*Infrared and Raman spectra of complexes of cationic gold clusters  $Au_n^+$  ( $n = 1-4$ ) and  $H_2S$  are computed using density functional theory. Intensities of  $H_2S$  spectral lines are significantly enhanced upon complex formation for both infrared and Raman spectra. Shifts in  $H_2S$  spectral lines are correlated with changes in geometries and binding energies of the complexes and charge transfer upon complex formation.*

**Keywords:** Infrared and Raman spectroscopy, gold clusters, hydrogen sulphide, complex formation.

## Introduction

Gold nanoclusters have unique physical and chemical

---

\* Author to whom correspondence should be addressed: [ihamilto@wlu.ca](mailto:ihamilto@wlu.ca)

properties that depend strongly on cluster size (1). To inhibit coalescence, sulphur-containing molecules are often used as surfactants because they form particularly stable gold nanocomplexes due to the strength of the gold-sulphur bond. The gold-sulphur bond has been used in nanodevices for attaching nanocrystals to surfaces or electrodes (2). Of relevance to the present paper, gold nanoparticles have been used for surface enhanced Raman scattering studies with a variety of molecules acting as chromophores (3-5). Also of relevance are recent infrared multiphoton dissociation studies of complexes of small cationic gold clusters and carbon monoxide (6,7).

Sugawara *et al.* have initiated an experimental study of the reactivity of gold cluster cations with a variety of sulphur-containing molecules in the gas phase using Fourier-transform ion-cyclotron resonance (FT-ICR) mass spectrometry. They have recently published results for the reactions of  $Au_n^+$  with  $H_2S$  for  $n = 1-12$  (8). Motivated by this work, we characterized geometries and binding energies of the  $Au_n^+SH_2$  complexes for  $n=1-4$  (9). In this paper, we extend this work to characterize the infrared and Raman spectra of these complexes. Shifts in spectral lines are correlated with changes in geometries and binding energies of the complexes and charge transfer upon complex formation. We focus on the effect of the  $Au_n^+$  cluster on the infrared and Raman spectrum of  $H_2S$ .

## Procedure

The Gaussian 03 program package (10) was employed for all electronic structure calculations. Equilibrium structures were obtained from geometry optimizations,

and harmonic frequencies of these structures were computed using the analytical second-order derivatives method.

As in our previous study (9), density functional theory (DFT) was employed throughout. We used the B3P86 functional which combines the Becke three-parameter hybrid exchange functional (11) with the Perdew gradient-corrected correlation functional (12). Other gradient-corrected functionals such as PW91 can also give satisfactory results for coinage metals (13). For coinage metals in general, and gold in particular, it is essential to include relativistic effects (14), and we do so by employing the Stuttgart-Dresden relativistic effective core potential (15) in combination with the D95 (double zeta) basis set for H<sub>2</sub>S, which was extended to include polarizing functions. Other relativistic effective core potentials such as RECP can also give satisfactory results for coinage metals (13). The B3P86/SDD\*\* method which we employ was shown to give good results for complexes of Cu and Ag clusters with NH<sub>3</sub> (16).

## Results and Discussion

The geometries of Au<sub>*n*</sub><sup>+</sup> and H<sub>2</sub>S have been previously characterized (9). For *n* = 3 and 4, the gold cluster cations are planar, and the Au<sub>3</sub><sup>+</sup> cluster has D<sub>3h</sub> symmetry while the Au<sub>4</sub><sup>+</sup> cluster has D<sub>2h</sub> symmetry. For H<sub>2</sub>S, with C<sub>2v</sub> symmetry, the calculated H-S distance is 1.346 Å (experimental value 1.3455 (17)).

The geometries of Au<sub>*n*</sub><sup>+</sup>H<sub>2</sub>S have also been previously characterized (9). For all complexes, the S atom is bonded to a single Au atom, and the geometries of both Au<sub>*n*</sub><sup>+</sup> and H<sub>2</sub>S are only slightly perturbed. In going from *n* = 1 to 4, the H-S distance decreases from 1.358 to 1.355 to 1.353 and 1.353 Å, while the Au-S distance increases from 2.320 to 2.349 to 2.384 to 2.407 Å. Both these trends are indicative of weaker bonding between Au<sub>*n*</sub><sup>+</sup> and H<sub>2</sub>S as the cluster size increases, and, indeed, the binding energy ( $\Delta H_0$ ) of the complex decreases from 60.3 to 45.5 to 39.3 to 34.7 kcal/mol for this sequence. This can be understood on purely electrostatic grounds: as the cluster size increases, the charge per Au atom decreases, and the attraction between the Au and S atoms is correspondingly smaller.

It is useful to characterize changes in the electron density distributions upon complex formation by examining changes in atomic charges of S and the Au bonded to S. We employ Mulliken charges, as they are

Table 1: Vibrations of H<sub>2</sub>S and selected vibrations of Au<sub>*n*</sub><sup>+</sup> and Au<sub>*n*</sub><sup>+</sup>SH<sub>2</sub>; mode (using Herzberg ordering), description, frequency in cm<sup>-1</sup>, IR intensity in km/mol and Raman intensity in Å<sup>4</sup>/amu.

Species	Mode	Description	Frequency	IR Intensity	Raman Intensity	
H <sub>2</sub> S	v <sub>1</sub>	asym str	2731	2.0	88.7	
	v <sub>2</sub>	sym str	2711	0.8	126.2	
	v <sub>3</sub>	bend	1218	1.7	38.2	
Au <sub>2</sub> <sup>+</sup>	v <sub>1</sub>	Au-Au str	140	0.0	4.8	
Au <sub>3</sub> <sup>+</sup>	v <sub>1</sub>	breathing	172	0.0	9.5	
Au <sub>4</sub> <sup>+</sup>	v <sub>1</sub>	breathing	156	0.0	12.5	
Au <sup>+</sup> SH <sub>2</sub>	v <sub>1</sub>	asym str	2652	42.5	77.7	
	v <sub>2</sub>	sym str	2635	46.0	160.1	
	v <sub>3</sub>	bend	1202	2.5	17.6	
	v <sub>5</sub>	sym H <sub>2</sub> S tilt	649	13.3	2.4	
	v <sub>6</sub>	Au-S str	298	2.1	3.6	
	Au <sub>2</sub> <sup>+</sup> SH <sub>2</sub>	v <sub>1</sub>	asym str	2669	27.0	89.6
Au <sub>3</sub> <sup>+</sup> SH <sub>2</sub>	v <sub>2</sub>	sym str	2653	40.1	241.0	
	v <sub>3</sub>	bend	1207	3.8	18.9	
	v <sub>5</sub>	sym H <sub>2</sub> S tilt	601	11.3	15.9	
	v <sub>6</sub>	Au-S str	284	0.0	9.2	
	v <sub>7</sub>	Au-Au str	129	1.7	1.2	
	Au <sub>4</sub> <sup>+</sup> SH <sub>2</sub>	v <sub>1</sub>	asym str	2682	21.6	85.2
	Au <sub>4</sub> <sup>+</sup> SH <sub>2</sub>	v <sub>2</sub>	sym str	2665	30.3	212.6
v <sub>3</sub>		bend	1207	5.7	16.0	
v <sub>5</sub>		sym H <sub>2</sub> S tilt	560	8.9	4.6	
v <sub>6</sub>		Au-S str	264	0.4	4.9	
v <sub>7</sub>		breathing	169	0.1	9.3	
v <sub>10</sub>		H <sub>2</sub> S rock	66	25.8	1.1	
Au <sub>4</sub> <sup>+</sup> SH <sub>2</sub>		v <sub>1</sub>	asym str	2686	19.5	77.5
	v <sub>2</sub>	sym str	2668	28.0	210.9	
	v <sub>3</sub>	bend	1203	7.2	11.0	
	v <sub>5</sub>	sym H <sub>2</sub> S tilt	545	10.4	6.1	
	v <sub>6</sub>	Au-S str	251	1.0	3.4	
	v <sub>7</sub>	breathing	149	0.2	13.7	
	v <sub>13</sub>	H <sub>2</sub> S rock	45	20.0	0.7	

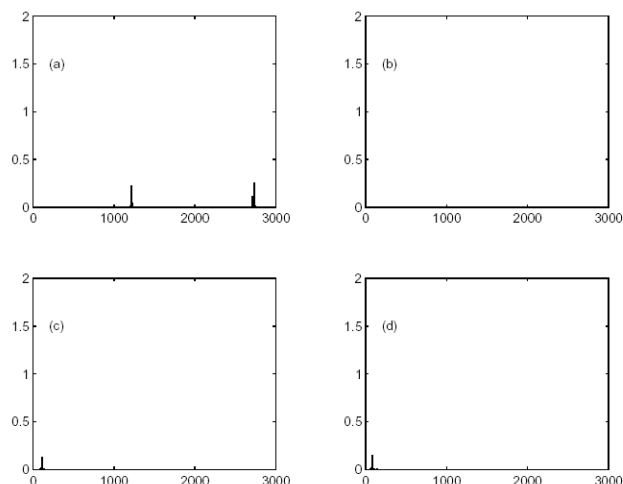


Figure 1. IR spectra for (a)  $\text{H}_2\text{S}$ , (b)  $\text{Au}_2^+$ , (c)  $\text{Au}_3^+$  and (d)  $\text{Au}_4^+$ . Frequencies in  $\text{cm}^{-1}$  and integrated intensities in  $\text{km/mol}$ .

widely used and have been employed for other cationic transition metal complexes (18), but, rather than reporting absolute charges which have well-known problems with basis set dependence, we report charge shifts. Upon complex formation, the S charge increases by 0.21, 0.13, 0.09 and 0.09 for  $n = 1$  to 4, and, for the same sequence, the Au charge decreases by 0.46, 0.25, 0.12 and 0.05. This trend of decreasing charge transfer is consistent with the trends of decreasing  $\text{Au}_n^+\text{SH}_2$  binding energy, increasing Au-S distance and decreasing H-S distance noted above.

We now consider the IR and Raman spectra of  $\text{H}_2\text{S}$ ,  $\text{Au}_n^+$  and  $\text{Au}_n^+\text{SH}_2$ . Our results for the vibrations of  $\text{H}_2\text{S}$  and selected vibrations of  $\text{Au}_n^+$  and  $\text{Au}_n^+\text{SH}_2$  are summarized in Table 1.

The IR spectrum of  $\text{H}_2\text{S}$  is well-known experimentally (19). The calculated vibrations of  $\text{H}_2\text{S}$  (with experimental values in parenthesis) are asymmetric stretch at 2731 (2627), symmetric stretch at 2711 (2615) and bend at 1218 (1183)  $\text{cm}^{-1}$ . Calibration with experiment would therefore require scaling by a factor of approximately 0.96, which is typical of calculated values (which neglect potential terms beyond quadratic). The calculated IR intensities are 2.0, 0.8 and 1.7  $\text{km/mol}$  for the asymmetric stretch, symmetric stretch and bend. Thus the asymmetric stretch is the most intense IR vibration. The calculated IR spectrum of  $\text{H}_2\text{S}$  is shown in Figure 1(a). For  $\text{Au}_n^+$ , the calculated vibrations are low frequency in the 10-160  $\text{cm}^{-1}$  range, and the calculated IR spectra for  $n = 2$ -

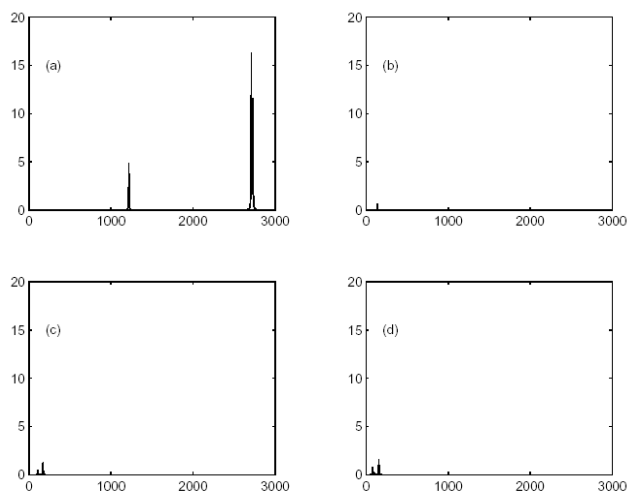


Figure 2. Raman spectra for (a)  $\text{H}_2\text{S}$ , (b)  $\text{Au}_2^+$ , (c)  $\text{Au}_3^+$  and (d)  $\text{Au}_4^+$ . Frequencies in  $\text{cm}^{-1}$  and integrated intensities in  $\text{Å}^4/\text{amu}$ .

4 are shown in Figure 1(b)-(d). All calculated IR intensities are very small (and zero for  $\text{Au}_2^+$ , which is included for completeness).

Conventional IR spectroscopy of gas phase ions is difficult due to low ion densities, and, to date, matrix isolation has been the technique of choice (20). Using matrix isolation or specialized techniques (such as velocity modulation), high resolution gas phase IR spectra have been obtained for cations such as  $\text{NCCN}^+$  (21) and  $\text{H}_3\text{O}^+$  (22), but these studies are far from routine.

The Raman spectrum of  $\text{H}_2\text{S}$  is well known experimentally, and Raman spectroscopy has recently been used to detect  $\text{H}_2\text{S}$  in low concentrations in desulphurized natural gas samples (23). The calculated Raman intensities are 88.7, 126.2 and 38.2  $\text{Å}^4/\text{amu}$  for the asymmetric stretch, symmetric stretch and bend. Thus the symmetric stretch is the most intense Raman vibration. The calculated Raman spectrum of  $\text{H}_2\text{S}$  is shown in Figure 2(a). For  $\text{Au}_n^+$ , the calculated Raman spectra for  $n = 2$  to 4 are shown in Figure 2(b)-(d). Most calculated Raman intensities are small, but, for  $n = 3$  and 4, the “breathing” mode at 172 and 156  $\text{cm}^{-1}$  is visible in Figures 2(c) and (d).

We now consider results for the vibrations of  $\text{Au}_n^+\text{SH}_2$ . The above comments regarding the difficulty of conventional IR spectroscopy of gas phase ions apply, of course, to ionic complexes. Besides the techniques noted above, infrared multiple photon dissociation (IRMPD) employing a fixed-frequency IR laser

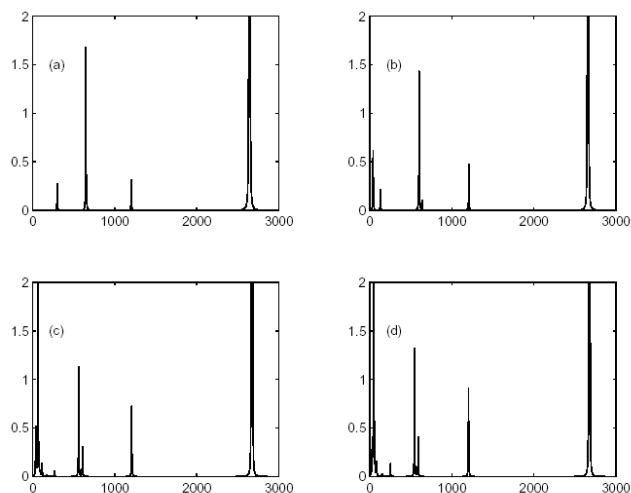


Figure 3. IR spectra for (a)  $\text{Au}^+\text{SH}_2$ , (b)  $\text{Au}_2^+\text{SH}_2$ , (c)  $\text{Au}_3^+\text{SH}_2$  and (d)  $\text{Au}_4^+\text{SH}_2$ .

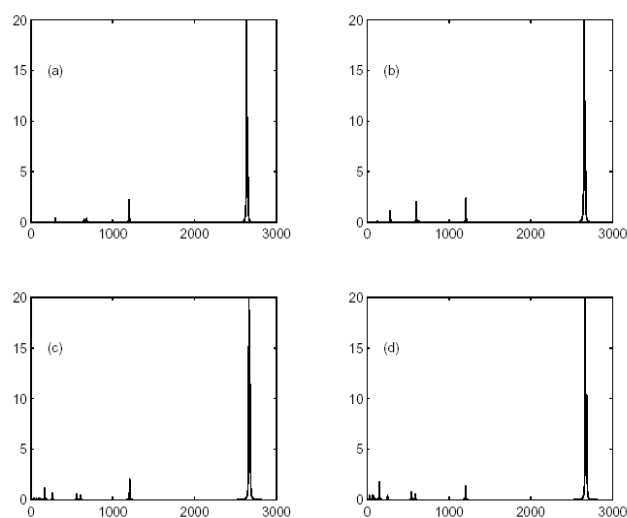


Figure 4. Raman spectra for (a)  $\text{Au}^+\text{SH}_2$ , (b)  $\text{Au}_2^+\text{SH}_2$ , (c)  $\text{Au}_3^+\text{SH}_2$  and (d)  $\text{Au}_4^+\text{SH}_2$ .

combined with an optical parametric oscillator (to shift the wavelength of the IR radiation) has been used to obtain IR spectra of either trapped ionic complexes (24,25) or mass-selected ionic complexes injected into an octopole ion guide (26,27). Of immediate relevance to the present paper are IRMPD studies of  $\text{Au}_n^+\text{CO}$  (6,7). We note that free electron lasers (FEL) provide a reliable broad-band light source for IRMPD studies (28), and IR spectroscopy of gas phase ions employing FEL may be more prevalent in the future.

The calculated IR spectra of  $\text{Au}_n^+\text{SH}_2$  for  $n = 1$  to 4 are shown in Figure 3(a)-(d), and the calculated Raman spectra are shown in Figure 4(a)-(d). The  $\text{H}_2\text{S}$  lines are

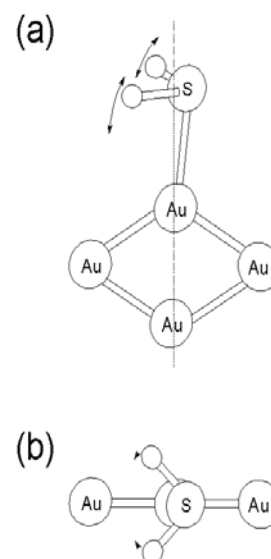


Figure 5. Symmetric  $\text{H}_2\text{S}$  tilt motion for  $\text{Au}_4^+\text{SH}_2$ ; (a) over plane of  $\text{Au}_4^+$  and (b) in plane of  $\text{Au}_4^+$ .

clearly visible in these spectra, and the most striking observation is that the intensity of these lines is significantly enhanced, particularly in the IR spectra. Upon complex formation, the IR intensity of the  $\text{H}_2\text{S}$  asymmetric stretch increases by a factor of 10-20, while the IR intensity of the  $\text{H}_2\text{S}$  symmetric stretch increases by a factor of 30-50, making it the most intense IR vibration. Overall, the Raman intensities of the  $\text{H}_2\text{S}$  asymmetric and symmetric stretch also increase, but by less than a factor of 2. In going from  $n = 1$  to 4, the asymmetric stretch is red shifted by 79, 62, 49 and 45  $\text{cm}^{-1}$ , while the symmetric stretch is red shifted by 76, 58, 46 and 43  $\text{cm}^{-1}$ . These shifts correlate with decreasing S-H distances which, in turn, correlate with increasing Au-S distances and decreasing Au-SH<sub>2</sub> binding energies. The shifts in the asymmetric and symmetric stretch lines could therefore be used for determination of cluster size in the complex.

Of the 3-6 additional vibrations due to the formation of the  $\text{Au}_n^+\text{SH}_2$  complex, the Au-S stretch may be most characteristic of the complex. The Au-S stretch decreases as the cluster size increases, which is consistent with changes in the Au-S distance noted above. The Au-S stretch is at 298, 284, 264 and 251  $\text{cm}^{-1}$  for  $n = 1$  to 4 but, unfortunately, the IR intensity is low. For the  $\text{Au}_n^+\text{SH}_2$  complexes, there is an intermediate-frequency mode, which we call the symmetric  $\text{H}_2\text{S}$  tilt, that involves symmetric motion of the hydrogen atoms parallel to the plane of the Au atoms (for  $n = 3$  and 4). This motion is shown in Figure 5 for  $\text{Au}_4^+\text{SH}_2$ . The symmetric  $\text{H}_2\text{S}$  tilt,

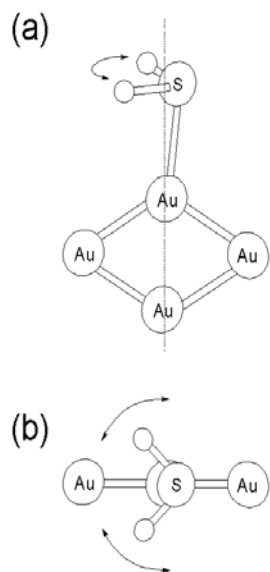


Figure 6.  $\text{H}_2\text{S}$  rock motion for  $\text{Au}_4^+\text{SH}_2$ ; (a) over plane of  $\text{Au}_4^+$  and (b) in plane of  $\text{Au}_4^+$ .

which is at 649, 601, 560 and  $545\text{ cm}^{-1}$  for  $n = 1, 2, 3$  and 4, has much higher IR intensity than the Au-S stretch (more than 10 times higher for  $n = 3$  and 4) and is easily seen in Figure 3(a)-(d). For  $n = 3$  and 4, there is a low-frequency mode that we call the  $\text{H}_2\text{S}$  rock, which involves back and forth motion of the hydrogen atoms perpendicular to the plane of the Au atoms and a resultant alternation of this component of the dipole moment. This motion is shown in Figure 6 for  $\text{Au}_4^+\text{SH}_2$ . The  $\text{H}_2\text{S}$  rock, which is at 66 and  $45\text{ cm}^{-1}$  for  $n = 3$  and 4, has even higher IR intensity than the symmetric  $\text{H}_2\text{S}$  tilt and is easily seen in Figures 3(c) and (d). The shifts for both the symmetric  $\text{H}_2\text{S}$  tilt and  $\text{H}_2\text{S}$  rock correlate with changes in geometries and binding energies of the complexes noted above, and thus these vibrations could also be used for determination of cluster size in the complex.

In summary, we have computed infrared and Raman spectra for complexes of small cationic gold clusters and hydrogen sulphide and observed that the intensities  $\text{H}_2\text{S}$  spectral lines are significantly enhanced upon complex formation, particularly for the infrared spectra. Also, two of the additional vibrations due to formation of the  $\text{Au}_n^+\text{SH}_2$  complex are relatively intense in the infrared spectra. Shifts in these three sets of spectral lines are correlated with changes in geometries and binding energies of the complexes, as well as charge transfer upon complex formation. Despite the strong Au-S bond,  $\text{H}_2\text{S}$  can therefore act as a chromophore to determine

cluster size in the  $\text{Au}_n^+\text{SH}_2$  complex. This is consistent with the observation that CO can act as a chromophore to determine cluster size in the  $\text{Au}_n^+\text{CO}$  complex (6,7). Unfortunately, there are no experimental results for the vibrations of  $\text{Au}_n^+\text{SH}_2$ . However, zero kinetic energy (ZEKE) spectroscopy has been employed to determine low-frequency vibrations for the cationic copper and silver-ammonia (29,30) and copper-pyridine (31) complexes. The ionization energy of gold is significantly higher but, if an electronically excited state of  $\text{AuSH}_2$  could be found, it might be possible to obtain its ZEKE spectrum using two photon ionization (32).

### Acknowledgements

I.P.H. thanks NSERC, SHARCNET and Wilfrid Laurier University for support and Ko-ichi Sugawara for helpful discussions. An earlier version of this work was presented as a talk at ICASS 2004 in Halifax.

### References

1. P. Schwerdtfeger, *Angew. Chem. Int. Ed.*, **42**, 1892 (2003).
2. Z. Hens, D.V. Tallapin, H. Weller and D. Vanmaekelbergh, *Appl. Phys. Lett.*, **81**, 4245 (2002).
3. N. Felidj, J. Aubard, G. Levi, J. R. Krenn, A. Hohenau, G. Schider, A. Leitner and F. R. Aussenegg, *App. Phys. Lett.*, **82**, 3095 (2003).
4. A. Pal, T. Pal, D.L. Stokes and T. Vo-Dinh, *Curr. Sci.*, **84**, 1342 (2003).
5. H. Zhao, B. Yuan and X. Dou, *J. Opt. A: Pure Appl. Opt.*, **6**, 900 (2004).
6. R. Rousseau, G. Dietrich, S. Kruckeberg, K. Lutzenkirchen, D. Marx, L. Schweikhard and C. Walther, *Chem. Phys. Lett.*, **295**, 41 (1998).
7. G. Dietrich, S. Kruckeberg, K. Lutzenkirchen, L. Schweikhard and C. Walther, *J. Chem. Phys.*, **112**, 752 (2000).
8. K. Sugawara, F. Sobott and A.B. Vakhtin, *J. Chem. Phys.*, **118**, 7808 (2003).
9. I.P. Hamilton, *Chem. Phys. Lett.*, **390**, 517 (2004).
10. *Gaussian 03, Revision A.1*, M. J. Frisch, G.W. Trucks, H.B. Schlegel, G.E. Scuseria, M.A. Robb, J.R. Cheeseman, J.A. Montgomery, Jr., T. Vreven, K.N. Kudin, J.C. Burant, J.M. Millam,

- S.S. Iyengar, J. Tomasi, V. Barone, B. Mennucci, M. Cossi, G. Scalmani, N. Rega, G.A. Petersson, H. Nakatsuji, M. Hada, M. Ehara, K. Toyota, R. Fukuda, J. Hasegawa, M. Ishida, T. Nakajima, Y. Honda, O. Kitao, H. Nakai, M. Klene, X. Li, J.E. Knox, H.P. Hratchian, J.B. Cross, C. Adamo, J. Jaramillo, R. Gomperts, R.E. Stratmann, O. Yazyev, A.J. Austin, R. Cammi, C. Pomelli, J.W. Ochterski, P.Y. Ayala, K. Morokuma, G.A. Voth, P. Salvador, J.J. Dannenberg, V.G. Zakrzewski, S. Dapprich, A.D. Daniels, M.C. Strain, O. Farkas, D.K. Malick, A.D. Rabuck, K. Raghavachari, J.B. Foresman, J.V. Ortiz, Q. Cui, A.G. Baboul, S. Cli.ord, J. Cioslowski, B.B. Stefanov, G. Liu, A. Liashenko, P. Piskorz, I. Komaromi, R.L. Martin, D.J. Fox, T. Keith, M.A. Al-Laham, C.Y. Peng, A. Nanayakkara, M. Challacombe, P.M.W. Gill, B. Johnson, W. Chen, M.W. Wong, C. Gonzalez, and J.A. Pople, Gaussian, Inc., Pittsburgh PA (2003).
11. A.D. Becke, *J. Chem. Phys.*, **98**, 5648 (1993).
  12. J.P. Perdue, *Phys. Rev. B*, **33**, 8822 (1986).
  13. X. Wu, L. Senapati, S.K. Nayak, A. Selloni and M. Hajaligol, *J. Chem. Phys.*, **117**, 4010 (2002).
  14. R. Wesendrup, T. Hunt and P. Schwerdtfeger, *J. Chem. Phys.*, **112**, 9356 (2000).
  15. D. Andrae, U. Haussermann, M. Dolg, H. Stoll and H. Preuss, *Theor. Chim. Acta.*, **77**, 123 (1990).
  16. W.-T. Chan and R. Fournier, *Chem. Phys. Lett.*, **315**, 257 (1999).
  17. R.C. Weast Ed., “*CRC Handbook of Chemistry and Physics*,” CRC Press, Boca Raton (1988).
  18. C.A. Sharrad, G.E. Cavigliasso, R. Stranger and L.R. Gahan, *Dalton Trans.*, **8**, 1166 (2004).
  19. H.H. Nielsen and E.F. Barker, *Phys. Rev.*, **37**, 727 (1931).
  20. L. Andrews and M. Moskovits Eds., “*Chemistry and Physics of Matrix-Isolated Species*,” Elsevier, New York (1989).
  21. E. Riaplov, M. Wyss, J.P. Maier, M. Hochlaf and P. Rosmus, *Int. J. Mass Spectrom.*, 107 (2003).
  22. M.H. Begemann, C.S. Gudeman, J. Pfaff and R.J. Saykally, *Phys. Rev. Lett.*, **51**, 554 (1983).
  23. S.B. Hansen, R.W. Berg and E.H. Stenby, *Appl. Spectrosc.*, **55**, 55 (2001).
  24. D.M. Peiris, J.M. Riveros and J.R. Eyler, *Int. J. Mass Spectrom. Ion Processes*, **159**, 169 (1996).
  25. P. Ayotte, G.H. Weddle, J. Kim and M.A. Johnson, *J. Am. Chem. Soc.*, **91**, 7319 (1989).
  26. L.I. Yeh, M. Okumura, J.D. Myers, J.M. Price and Y.T. Lee, *J. Chem. Phys.*, **120**, 12361 (1998).
  27. O. Dopfer, D. Roth and J.P. Maier, *J. Am. Chem. Soc.*, **124**, 494 (2002).
  28. H. Piest, G. von Holden and G. Meißner, *J. Chem. Phys.*, **110**, 2010 (1999).
  29. J. Miyawaki, D.-S. Yang and K. Sugawara, *Chem. Phys. Lett.*, **372**, 627 (2003).
  30. J. Miyawaki and K. Sugawara, *J. Chem. Phys.*, **119**, 6539 (2003).
  31. J. Miyawaki and K. Sugawara, *Chem. Phys. Lett.*, **386**, 196 (2004).
  32. Ko-ichi Sugawara, private communication.